Journal of Power Sources 196 (2011) 1840–1846

Contents lists available at ScienceDirect

Journal of Power Sources

journal homepage: www.elsevier.com/locate/jpowsour

Order–disorder transformation and enhanced oxide-ionic conductivity of $(Sm_{1-x}Dy_x)_2Zr_2O_7$ ceramics

Xiao-Liang Xia, Zhan-Guo Liu, Jia-Hu Ouyang*

Institute for Advanced Ceramics, Department of Materials Science, Harbin Institute of Technology, Harbin 150001, China

ARTICLE INFO

Article history:
Received 23 July 2010
Received in revised form 5 September 2010
Accepted 20 September 2010
Available online 29 September 2010

Keywords:
Order
Disorder
Transformation
Solid electrolyte
Ionic conductivity

ABSTRACT

$(Sm_{1-x}Dy_x)_2Zr_2O_7$ $(0 \le x \le 1)$ ceramics are prepared by a solid state reaction process at 1973 K for 10 h in air. $(Sm_{1-x}Dy_x)_2Zr_2O_7$ $(0 \le x \le 0.3)$ ceramics exhibit a single phase of pyrochlore-type structure, while $(Sm_{1-x}Dy_x)_2Zr_2O_7$ $(0.5 \le x \le 1.0)$ possess a defective fluorite-type structure. The full width at half-maxima in the Raman spectra increases with increasing Dy content, which indicates that the degree of structural disorder increases as the Dy content increases. The ionic conductivity of $(Sm_{1-x}Dy_x)_2Zr_2O_7$ ceramics is investigated by impedance spectroscopy over a frequency range of 0.2 Hz to 8 MHz in the temperature range of 873–1173 K in air and hydrogen atmospheres, respectively. The ionic conductivity has a maximum near the phase boundary between the pyrochlore- and the defective fluorite-type phases under identical temperature levels. The ionic conductivity is determined by the degree of structural disorder or unit cell free volume, which is depending on the Dy content. As the ionic conductivity in the hydrogen atmosphere is almost the same as that obtained in air, the conduction of $(Sm_{1-x}Dy_x)_2Zr_2O_7$ is purely ionic with negligible electronic conduction.

1. Introduction

Pyrochlore-type oxides with the general formula, $A_2B_2O_7$ (A and B are metallic elements), are very important in both basic science research and engineering application [1]. They have attracted much attention in materials science due to their special structure and interesting physical, chemical properties such as semiconducting properties and ionic conductivity [2]. The intrinsic existence of anion vacancy enables pyrochlore-type oxides possess good oxide ion conductivity, and can be considered as a potential candidate as solid electrolytes for intermediate temperature solid oxide fuel cell (SOFC) applications [3]. The solid electrolytes are the heart of SOFC. Reducing the operation temperature of SOFC has stimulated many efforts to search for novel electrolytes [4]. Rare-earth zirconates have been of considerable interest as potential electrolytes for intermediate temperature SOFC due to their high ionic conductivity at relatively low temperatures [5–11]. The electrical conductivity of the pyrochlore phase $Sm_2Zr_2O_7$ was comparable to those of good oxide-ion conductors in low temperature region [7]. During the past decades, $Gd_2Zr_2O_7$ doped with rare earth cations like Nd, Sm, and Eu was widely investigated as potential electrolyte materials to further improve electrical conductivity [9–11]. The order–disorder transformation in a pyrochlore-type structure is quite interesting due to the occurrence of order–disorder transformation in both the anion and the cation arrangements. Modified pyrochlore oxides are of great interest in solid electrolytes due to their high oxide ion conductivity, which makes them suitable for applications in SOFC [12]. It has been found that electrical conductivity of pyrochlore-type materials is obviously higher than that of defective fluorite-type materials for doped $Sm_2Zr_2O_7$ ceramics in the temperature range of 723–1073 K [13,14]. However, the crystal structure and electrical conductivity of $(Sm_{1-x}Dy_x)_2Zr_2O_7$ ceramics have not been investigated in open literatures.

In the present paper, we prepare the $(Sm_{1-x}Dy_x)_2Zr_2O_7$ $(0 \le x \le 1.0)$ ceramics, in which the phase transformation of pyrochlore (order) to defective fluorite (disorder) is observed. The order–disorder transformation is studied by X-ray diffraction and Raman spectroscopy techniques. The objective of this work is to investigate the phase transformation and electrical behavior of the pyrochlore- and defective fluorite-type phases for $(Sm_{1-x}Dy_x)_2Zr_2O_7$ ceramics in detail.

2. Experimental procedure

$(Sm_{1-x}Dy_x)_2Zr_2O_7$ $(0 \le x \le 1.0)$ ceramics were prepared by a solid-state reaction process using Sm_2O_3, Dy_2O_3 (Grirem Advanced Materials Co. Ltd., China; purity ≥ 99.9%) and ZrO_2 (Nanbo Structure Ceramics Co. Ltd., China; purity ≥ 99.9%) powders as starting materials. All raw powders were calcined at 1173 K for 2 h to remove any adsorptive water in air before weighing. Samaria, zirconia

* Corresponding author. Tel.: +86 451 86414291; fax: +86 451 86414291.
E-mail address: ouyangjh@hit.edu.cn (J.-H. Ouyang).

0378-7753/$ – see front matter © 2010 Elsevier B.V. All rights reserved.
doi:10.1016/j.jpowsour.2010.09.056

and dysprosium oxide powders in appropriate molar ratios were mechanically mixed for 24 h. The dried powder mixtures were uniaxially molded at 20 MPa and then subjected to cold isostatic pressing at 280 MPa for 5 min. Finally, the compacts were sintered at 1973 K for 10 h in air to prepare dense bulk materials. The bulk density of as-sintered samples was measured by the Archimedes principle. The theoretical density was calculated using molecular weight in a unit cell and lattice parameters.

The phases of sintered ceramics were characterized by an X-ray diffractometer (Rigaku, D/MAX 2200VPC, Japan) with Cu Kα radiation. Continuous scans were used for qualitative phase identification in the 2θ range of 10–90° at a scan rate of 4° min^{-1}, whereas slow step-scans with a step width of 0.02° and a step time of 3 s were carried out on the diffraction peak of $(3\,1\,1)_F/(6\,2\,2)_{Py}$ in the 2θ range of 56–60° to determine the shifts of the X-ray spectra. The lattice parameters were estimated with silicon as the external standard. The microstructure of bulk ceramics was observed by a scanning electron microscope (FEI Quanta 200F, the Netherlands). The specimens were ground with abrasive papers and were then polished with a 1 μm diamond paste. Finally, the specimens were thermally etched at 1923 K for 1 h in air and a thin carbon coating was evaporated onto the specimens for electrical conductivity before SEM observations. The Raman spectra were recorded using the 458 nm line from an argon ion laser by Raman system (JY Horiba HR800, France). The laser power of about 5 mW was focused to a spot of approximate 2 μm, and a standard 50× objective lens was used for the collection of the back-scattered Raman signal. The Raman signal was collected for 20 s for all specimens. The instrument was carefully calibrated by single-crystal Si before measurements.

Cylindrical pellet-form specimens of 8 mm in diameter and about 1 mm in thickness were machined. Platinum paste was painted as electrodes on both sides of each pellet and then fired at 1223 K for 2.5 h in air to ensure a good contact with pellets. Platinum wires were attached on the Pt electrodes for measurements. The conductivity of the pellets was measured as a function of temperature from 873 to 1173 K by a four-probe method. The electrical conductivity was investigated by impedance spectroscopy in the automated setup assembled on the frequency response analyzer SI 1260 (Solartron Instruments, UK) in air and hydrogen atmospheres, respectively. The ZView 3.1c and ZPlot 3.1c softwares associated with Solartron instrument were used to analyze the impedance spectra.

3. Results and discussion

The relative densities of $(Sm_{1-x}Dy_x)_2Zr_2O_7$ ceramics are in the range of 88.1–96.3%, as shown in Table 1. Fig. 1 shows

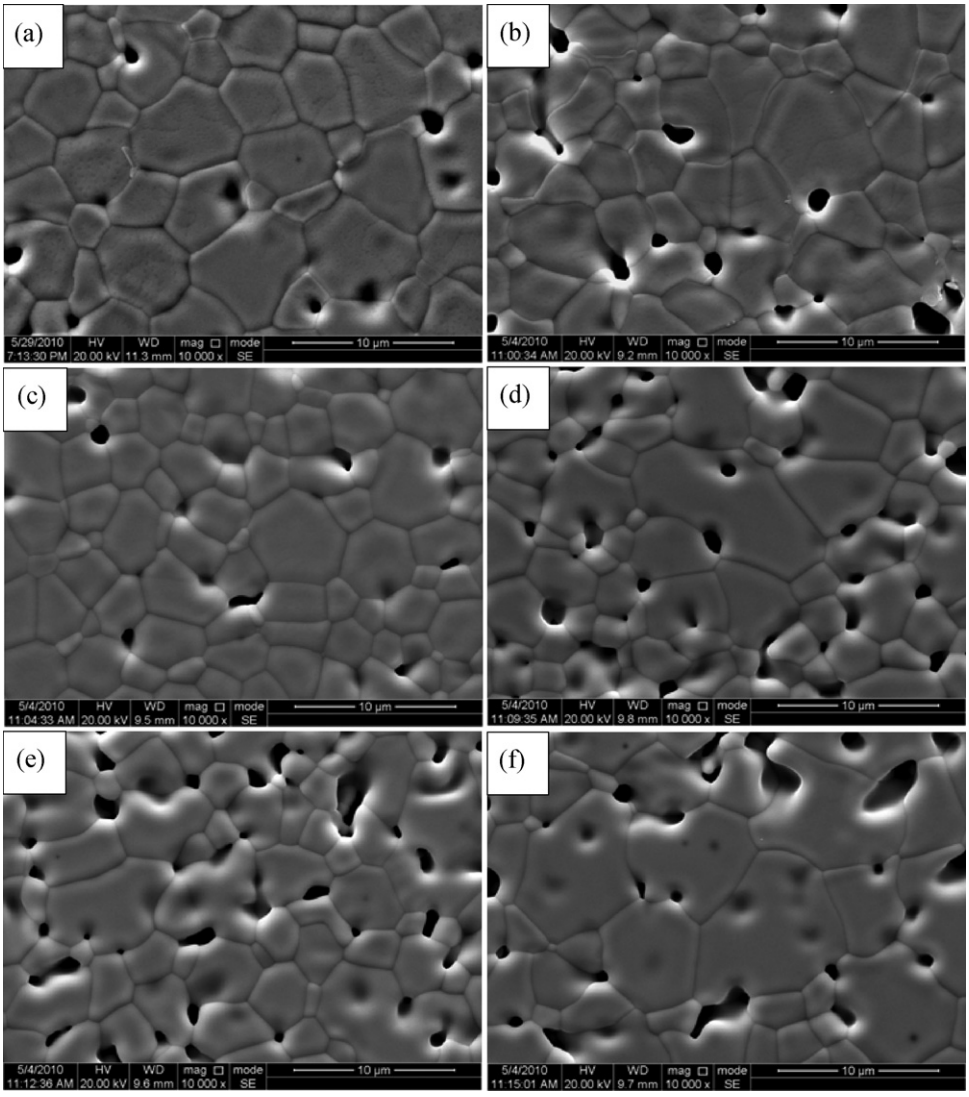

Fig. 1. Microstructure of $(Sm_{1-x}Dy_x)_2Zr_2O_7$ ceramics sintered at 1973 K for 10 h in air: (a) $x = 0$, (b) $x = 0.1$, (c) $x = 0.3$, (d) $x = 0.5$, (e) $x = 0.7$ and (f) $x = 1.0$.

Table 1
Relative densities of $(Sm_{1-x}Dy_x)_2Zr_2O_7$ ceramics used in this investigation.

Ceramic materials	Relative density (%)
$Sm_2Zr_2O_7$	96.3
$(Sm_{0.9}Dy_{0.1})_2Zr_2O_7$	92.6
$(Sm_{0.7}Dy_{0.3})_2Zr_2O_7$	93.7
$(Sm_{0.5}Dy_{0.5})_2Zr_2O_7$	89.1
$(Sm_{0.3}Dy_{0.7})_2Zr_2O_7$	88.1
$Dy_2Zr_2O_7$	90.0

the microstructure of $(Sm_{1-x}Dy_x)_2Zr_2O_7$ $(0 \le x \le 1.0)$ ceramics sintered at 1973 K for 10 h in air. Apparently, there are some small pores in $(Sm_{1-x}Dy_x)_2Zr_2O_7$ ceramics. The average grain size of $(Sm_{1-x}Dy_x)_2Zr_2O_7$ ceramics is several micrometers, and is almost independent of the Dy content. The grain boundaries of $(Sm_{1-x}Dy_x)_2Zr_2O_7$ ceramics are clean, and no other phases are found at the grain boundaries.

Fig. 2(a) reveals the XRD patterns of $(Sm_{1-x}Dy_x)_2Zr_2O_7$ $(0 \le x \le 1.0)$ ceramics sintered at 1973 K for 10 h in air. Clearly, all of compositions have a single cubic phase. $(Sm_{1-x}Dy_x)_2Zr_2O_7$ ($x = 0$, 0.1, 0.3) ceramics exhibit an ordered pyrochlore-type structure, which is characterized by the presence of typical superstructure diffraction peaks at the 2θ values of 14° (1 1 1), 28° (3 1 1), 37° (3 3 1), 45° (5 1 1) and 51° (5 3 1) using Cu Kα radiation [15,16]. With the decrease in $r(A^{3+})/r(B^{4+})$ of $A_2B_2O_7$ system, the structure exhibits a defective fluorite-type structure, and the superstructure diffraction peaks disappear, as illustrated for $(Sm_{1-x}Dy_x)_2Zr_2O_7$ ($x = 0.5$, 0.7, 1.0) in Fig. 2(a). The ordered pyrochlore-type structure is favored when the cation radius ratio of $r(A^{3+})/r(B^{4+})$ is at the range of 1.46–1.78 [e.g., $Sm_2Zr_2O_7$, $r(A^{3+})/r(B^{4+}) = 1.50$]. However, if the radius ratio is less than 1.46, a defective fluorite-type structure is formed [e.g., $Dy_2Zr_2O_7$, $r(A^{3+})/r(B^{4+}) = 1.43$]. In certain pyrochlore-type ceramics, an increase in cation disorder is observed with decreasing $r(A^{3+})/r(B^{4+})$, which is also accompanied by anion disorder as the vacant 8*b* site becomes progressively occupied by a partial removal of oxide from 48*f* to 8*a* site [17]. The ionic radius of Zr^{4+} is 0.72 Å in a six-fold coordination, while the ionic radius of Sm^{3+} and Dy^{3+} are 1.079 and 1.027 Å in an eight-fold coordination, respectively [18]. The values of $r(A^{3+})/r(B^{4+})$ for $(Sm_{1-x}Dy_x)_2Zr_2O_7$ ($x = 0$, 0.1, 0.3) ceramics are higher than 1.46; therefore, they exhibit an ordered pyrochlore-type structure; while the values of $r(A^{3+})/r(B^{4+})$ for $(Sm_{1-x}Dy_x)_2Zr_2O_7$ ($x = 0.5$, 0.7, 1.0) ceramics are clearly lower than 1.46, thus, a defective fluorite-type structure is favored.

Fig. 2(b) shows the XRD patterns of $(Sm_{1-x}Dy_x)_2Zr_2O_7$ ceramics in the 2θ range of 56–60°. The $(3\,1\,1)_F/(6\,2\,2)_{Py}$ peak of $(Sm_{1-x}Dy_x)_2Zr_2O_7$ ceramics shifts gradually to the high angle region with increasing Dy content, which is related to the change in average ionic radius of *A* site including $(1-x)Sm^{3+}$ and xDy^{3+} cations. The lattice parameters as a function of the Dy content are illustrated in Fig. 2(c). An approximately linear decrease in lattice parameters for $(Sm_{1-x}Dy_x)_2Zr_2O_7$ ceramics is observed with increasing Dy content from $x = 0$ to $x = 1.0$, which agrees well with Vegard's law. This is attributed to the substitution of small Dy^{3+} cations for large Sm^{3+} in an eight-fold coordination.

Raman spectroscopy was carried out to verify the degree of structural order/disorder in $(Sm_{1-x}Dy_x)_2Zr_2O_7$ ceramics over the frequency range of 200–800 cm^{-1}. Fig. 3 shows the Raman spectra of $(Sm_{1-x}Dy_x)_2Zr_2O_7$ ceramics with different Dy contents. Apparently, with increasing Dy content doped into $Sm_2Zr_2O_7$, the widths of different Raman modes at about 305, 390 and 525 cm^{-1} increase till they are broadened at the composition of $(Sm_{0.5}Dy_{0.5})_2Zr_2O_7$ in this investigation. Cubic pyrochlore (space group *Fd3m*) has six Raman active modes distributed as $A_{1g} + E_g + 4F_{2g}$ [19]. From Fig. 3, Raman spectra are dominated by three intense bands at about 305, 390 and 525 cm^{-1}, which are assigned to the O–Sm(Dy)–O bending, Zr–O stretch, and Sm(Dy)–O stretch modes, respectively. One of obvious characteristics is that the intensity of the pyrochlore-type Raman mode at 305 cm^{-1} gradually decreases with increasing Dy content. The change in widths of this mode is shown in Fig. 4. The full width at half-maximum (FWHM) of peaks around 305 cm^{-1} increases with increasing Dy content (Fig. 4). This is closely related with the cationic antisite disorder resulting in the oxygen disorder, which increases the width of Raman lines [20]. In general, the FWHM of the peaks increases as a result of the increase in the degree of structural disorder [21]. Therefore, the degree of structural disorder increases with increasing Dy content, which is in accordance with the XRD results.

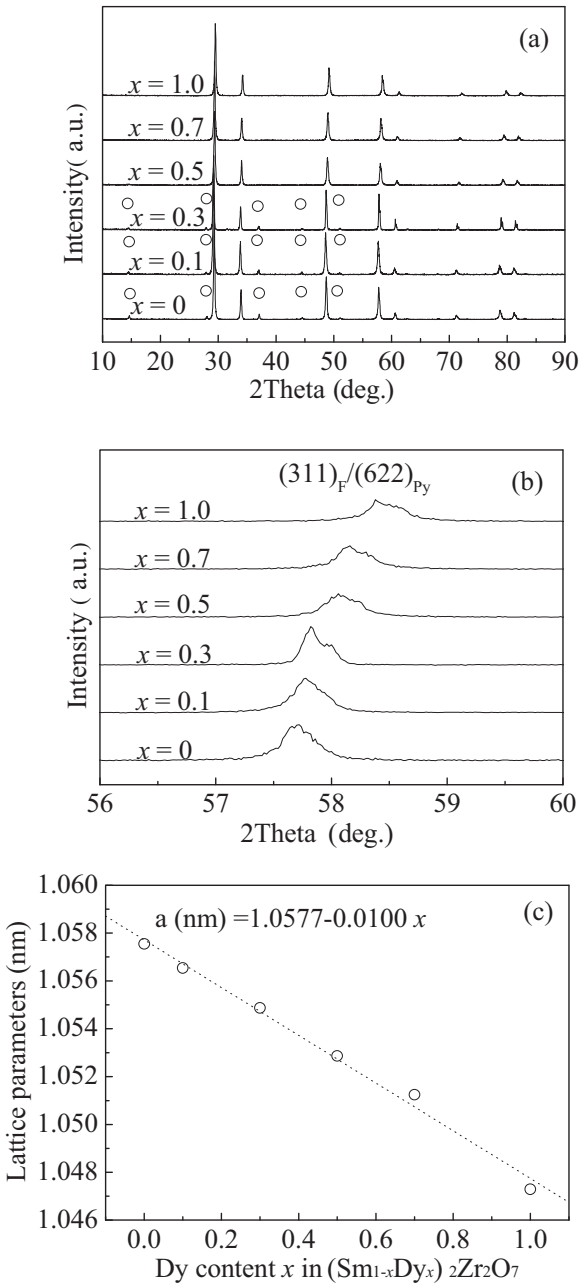

Fig. 2. XRD patterns and lattice parameters of $(Sm_{1-x}Dy_x)_2Zr_2O_7$ ceramics: (a) in the 2θ range of 10–90°, (b) $(311)_F/(622)_{Py}$ peak in the 2θ range of 56–60° and (c) lattice parameters. The symbol (○) represents the superstructure peaks.

In general, ZView software is a convenient tool to analyze the impedance spectra by the equivalent circuit method. In the investigation, the separate resistance along with the value of capacitance

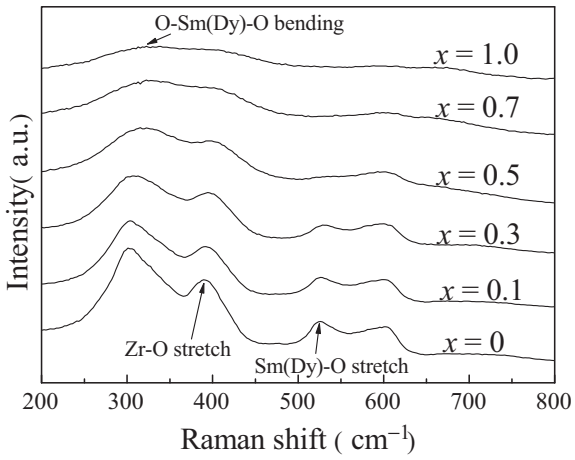

Fig. 3. Raman spectra of $(Sm_{1-x}Dy_x)_2Zr_2O_7$ ceramics doped with different Dy contents.

in the circuit was evaluated by analyzing the impedance spectra using ZView 3.1c software associated with Solartron Instrument. Fig. 5 shows typical complex impedance plots and corresponding equivalent electrical circuit for selected $(Sm_{1-x}Dy_x)_2Zr_2O_7$ ceramics at 873 K in air, where two main features are evident. From Fig. 5(a), capacitance values obtained for the high and low frequency arcs are 3.30×10^{-8} and 6.43×10^{-4} F cm^{-1} at 873 K, which corresponds to the grain boundary and electrode contributions for pyrochlore-type $(Sm_{0.7}Dy_{0.3})_2Zr_2O_7$, respectively. However, for defective fluorite-type $(Sm_{0.5}Dy_{0.5})_2Zr_2O_7$ ceramic, there is an instrumental or measurement artifact which is the grain resistance and should be added to the resistance of the first semicircle. Capacitance values obtained for the high and low frequency arcs are 5.55×10^{-11} and 7.98×10^{-4} F cm^{-1} as shown in Fig. 5(b), which corresponds to the grain and electrode contributions, respectively. As a solid electrolyte of SOFC, the electrical resistivity of the grain boundary may affect the total electrical conductivity. From Fig. 5(a), the grain and grain boundary contributions are manifested, which indicates that the total electrical conductivity is controlled by the grain and grain boundary contributions for the pyrochlore-type ceramics. However, only the grain contribution is clearly observed from Fig. 5(b), which suggests that the grain boundary contribution for total electrical conductivity is negligibly small in defective fluorite-type ceramics. So in the latter

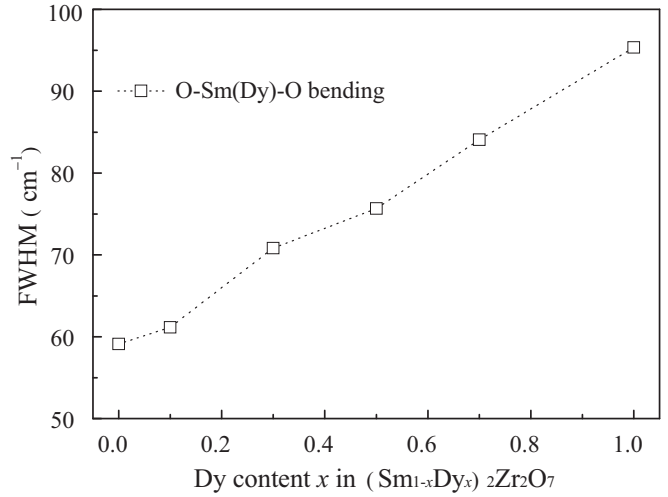

Fig. 4. The changes in widths of one Raman mode around 305 cm^{-1}, corresponding to O–Sm(Dy)–O bending, as a function of Dy content in $(Sm_{1-x}Dy_x)_2Zr_2O_7$ ceramics.

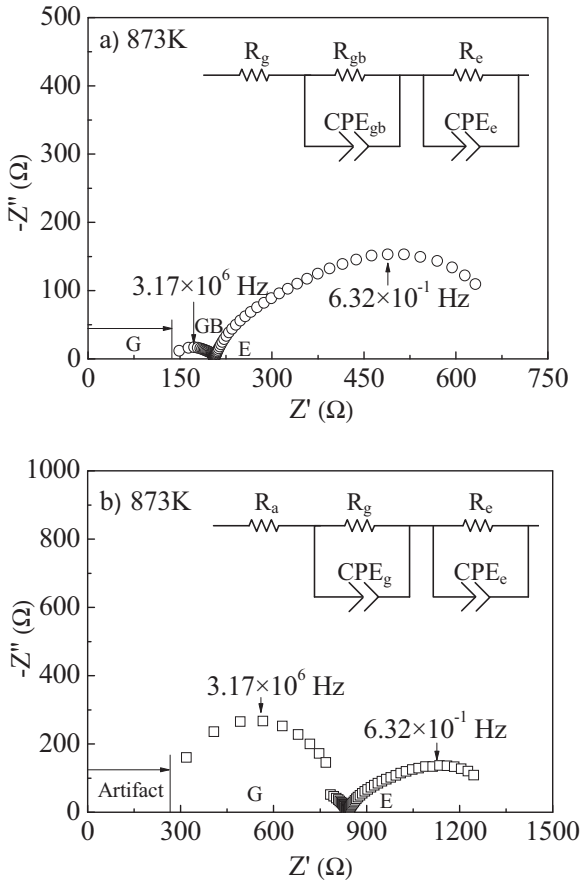

Fig. 5. Typical complex impedance plots and corresponding equivalent electrical circuit for selected $(Sm_{1-x}Dy_x)_2Zr_2O_7$ ceramics at 873 K in air: (a) $(Sm_{0.7}Dy_{0.3})_2Zr_2O_7$, (b) $(Sm_{0.5}Dy_{0.5})_2Zr_2O_7$. The artifact (a), grain (G), grain-boundary (GB) and electrode (E) contributions are indicated.

part, only the grain conductivity and total conductivity are discussed, whereas the grain boundary conductivity is not discussed by itself. At a given measurement temperature, a typical equivalent circuit model consisting of parallel resistance–capacitance was applied to fit the experimental data and reproduce impedance plots [22]. The measured data are also analyzed using a nonlinear least-squares-fit program, such as the well-known Equivalent Circuit (EQUIVCRT.PAS) [23] and almost the same results are found. Accordingly, the electrical conductivity σ of $(Sm_{1-x}Dy_x)_2Zr_2O_7$ ceramics can be easily calculated from resistance values R using the following equation:

$$\sigma = \frac{l}{RS} \tag{1}$$

where σ is electrical conductivity, R is resistance value, l is sample thickness, and S is electrode area of the sample surface. The temperature dependence of electrical conductivity with the Dy content can be analyzed by using an Arrhenius-type law with the following form:

$$\sigma T = \sigma_0 \exp\left(\frac{-E}{k_B T}\right) \tag{2}$$

where σ_0 is the pre-exponential factor, which is related to the concentration of mobile ions. E is the activation energy for oxide-ion conduction. k_B is the Boltzmann constant and T is the absolute temperature.

Fig. 6 presents the Arrhenius plots of the grain conductivity in air for $(Sm_{1-x}Dy_x)_2Zr_2O_7$ ceramics. The activation energy E_g and pre-exponential factor σ_{0g} of the grain conductivity for

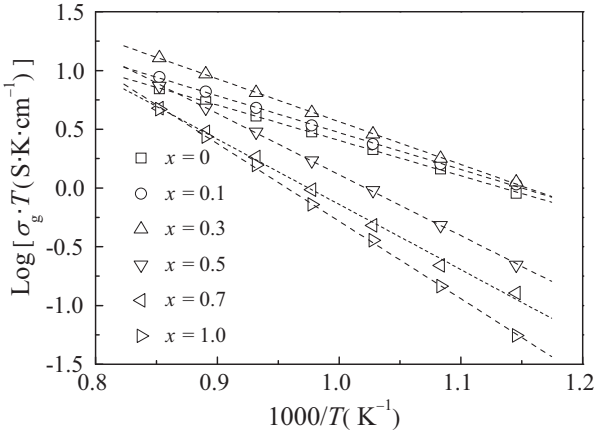

Fig. 6. Arrhenius plots of grain conductivity for $(Sm_{1-x}Dy_x)_2Zr_2O_7$ ceramics.

Table 2
Activation energy and pre-exponential factor of the grain conductivity for $(Sm_{1-x}Dy_x)_2Zr_2O_7$ ceramics.

Ceramics materials	Grain conductivity contribution	
	Activation energy E_g (eV)	Pre-exponential factor σ_{0g} (S K cm^{-1})
$Sm_2Zr_2O_7$	0.60	2.62×10^3
$(Sm_{0.9}Dy_{0.1})_2Zr_2O_7$	0.62	4.11×10^3
$(Sm_{0.7}Dy_{0.3})_2Zr_2O_7$	0.72	1.64×10^4
$(Sm_{0.5}Dy_{0.5})_2Zr_2O_7$	1.03	2.03×10^5
$(Sm_{0.3}Dy_{0.7})_2Zr_2O_7$	1.10	2.61×10^5
$Dy_2Zr_2O_7$	1.13	2.07×10^6

each composition are shown in Table 2. The activation energy E_g of the grain conduction for different pyrochlore-type phases of $Sm_2Zr_2O_7$, $(Sm_{0.9}Dy_{0.1})_2Zr_2O_7$ and $(Sm_{0.7}Dy_{0.3})_2Zr_2O_7$ are 0.6, 0.62 and 0.72 eV, respectively. However, the activation energy E_g of the grain conduction for different defective fluorite-type phases of $(Sm_{0.5}Dy_{0.5})_2Zr_2O_7$, $(Sm_{0.3}Dy_{0.7})_2Zr_2O_7$ and $Dy_2Zr_2O_7$ are 1.03, 1.10 and 1.13 eV, respectively, which are obviously higher than those of pyrochlore-type phases.

Fig. 7 shows the activation energy for $(Sm_{1-x}Dy_x)_2Zr_2O_7$ ceramics as a function of the Dy content. The activation energy first increases slowly with increasing Dy content in the pyrochlore phase region. However, the activation energy increases rapidly when subjected to the phase transformation from pyrochlore to defective fluorite, and then increases gradually with further increasing Dy content in the defective fluorite phase region. Yamamura et al. [24] confirmed that the unit cell free volume influenced the activation energy of electrical conductivity in the fluorite-type oxides. In order to understand the compositional change of the electrical conductivity in the present investigation, it is supposed that their discussion could also be applied to the present study as there exists only the change in lattice volume in $(Sm_{1-x}Dy_x)_2Zr_2O_7$ ceramics, whereas the oxygen vacancy concentration is kept constant. Fig. 8 shows the relationship between V_f/V_c values and the Dy content for $(Sm_{1-x}Dy_x)_2Zr_2O_7$ ceramics, where V_f means the unit cell free volume and V_c means the unit cell volume. Unit cell free volume (V_f) was calculated using the following form:

$$V_f = \left(\frac{a}{2}\right)^3 - \frac{4}{3}\pi[2(1-x)r_{Sm^{3+}}{}^3 + 2xr_{Dy^{3+}}{}^3 + 2r_{Zr^{4+}}{}^3 + 8r_{O^{2-}}{}^3 - r_{V_O}{}^3] \quad (3)$$

where a and x denote the lattice parameter of pyrochlore phase and the Dy content, and $r_{Sm^{3+}}$, $r_{Dy^{3+}}$, $r_{Zr^{4+}}$, $r_{O^{2-}}$ and r_{V_O} are the radius of the Sm^{3+}(1.079), Dy^{3+}(1.027), Zr^{4+}(0.720), oxide-ion(1.380) and oxygen vacancy(0.993 Å) [25], respectively.

From the estimation of unit cell free volume, V_f/V_c values decrease rapidly in the pyrochlore phase region, however; the activation energy for the grain conductivity gradually increases with increasing Dy content from $x = 0$ to 0.3. Therefore, the activation energy is not dominant by the unit cell free volume. The V_f/V_c values varied drastically at the phase boundary between the pyrochlore- and the defective fluorite-type structures, meanwhile, the corresponding activation energy for the grain conductivity obviously increased. Thus, the activation energy is dominated by the unit cell free volume.

Fig. 9(a) illustrates the grain conductivity of $(Sm_{1-x}Dy_x)_2Zr_2O_7$ ceramics as a function of the Dy content. From Fig. 9(a), the conductivity value first increases with increasing Dy content in the pyrochlore phase region, and exhibits the maximum value at the phase boundary between the pyrochlore- and defective fluorite-type phase regions, and then decreases with further increasing Dy content in the defective fluorite-type phase region. The pyrochlore-type $(Sm_{0.7}Dy_{0.3})_2Zr_2O_7$ shows the maximum conductivity value of 1.10×10^{-2} S cm^{-1} at 1173 K, which is lower than the value of M^{3+}-stabilized cubic zirconia (about 10^{-1} S cm^{-1} at identical temperature level). Clearly, the grain conductivity gradually increases with increasing the Dy content from $x = 0$ to 0.3 in the pyrochlore phase region. However, the grain conductivity decreases with increasing Dy content from $x = 0.3$ to 0.5, meanwhile, the structure changes from pyrochlore to defective fluorite phase. With further increasing Dy content from $x = 0.5$ to 1.0, the grain conduc-

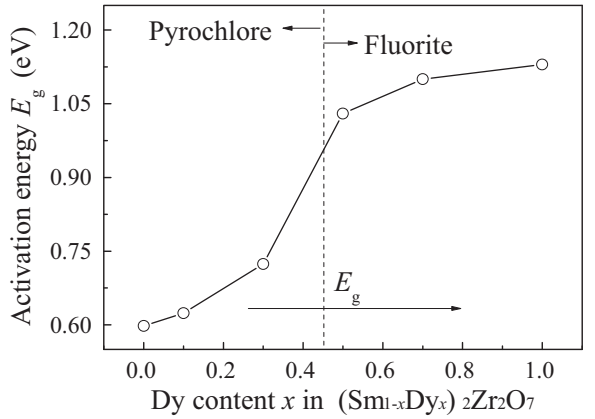

Fig. 7. Activation energy E_g of grain conductivity as a function of the Dy content for $(Sm_{1-x}Dy_x)_2Zr_2O_7$ ceramics.

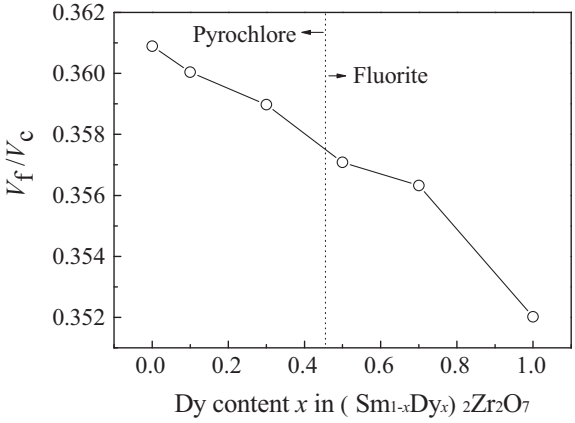

Fig. 8. The relationship between V_f/V_c values and the Dy content for $(Sm_{1-x}Dy_x)_2Zr_2O_7$ ceramics. V_f means the unit cell free volume and V_c means the unit cell volume.

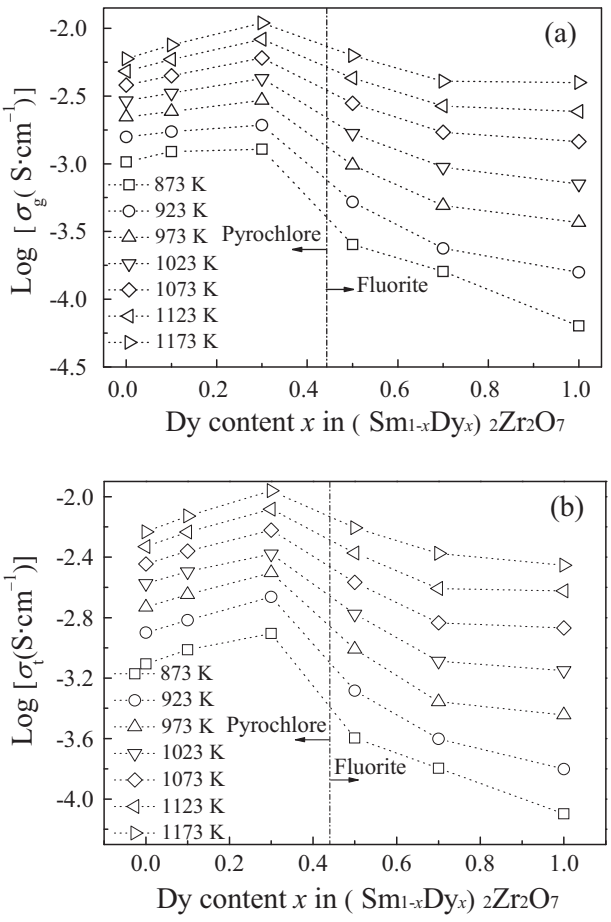

Fig. 9. Grain conductivity (σ_g) and total conductivity (σ_t) of $(Sm_{1-x}Dy_x)_2Zr_2O_7$ ceramics as a function of Dy content: (a) grain conductivity, (b) total conductivity.

tivity gradually decreases in the defective fluorite phase region. The value of total conductivity is more important than that of the grain conductivity for applications in solid oxide fuel cells (or any electrochemical device). Generally, the total ionic conductivity of materials is obtained by using the total resistance, which is obtained from the intersection of low frequency semicircle with Z'-axis. Fig. 9(b) represents the effect of increasing Dy content on total conductivity of $(Sm_{1-x}Dy_x)_2Zr_2O_7$ ceramics at different temperatures. Apparently, the total conductivity exhibits similar results to the grain conductivity with increasing Dy content, and is a little bit lower than grain conductivity. Therefore, the grain has major role in controlling the total ionic conductivity and conduction mechanisms for all $(Sm_{1-x}Dy_x)_2Zr_2O_7$ ceramics.

As discussed in the earlier part, Raman spectroscopy reveals that the degree of structural disorder gradually increases with increasing Dy content; meanwhile, the effective number of mobile oxide ions increases. As shown in Table 2, σ_{0g} slightly increases at $x = 0.1$ and increases about one order of magnitude at $x = 0.3$. The increase in σ_{0g} would lead to an increase in electrical conductivity; at the same time, the unit cell free volume for oxide-ion migration decreases as a result of small Dy^{3+} substitution for large Sm^{3+}. Consequently, the activation energy for oxide ion transport increases. However, the activation energy E_g shows no distinct change from $x = 0$ to $x = 0.3$ (Table 2). Thus, the increase in electrical conductivity from $x = 0$ to $x = 0.3$ is caused by an increase in the degree of structural disorder. With further increasing Dy content from $x = 0.3$ to 0.5, the structural transformation from pyrochlore (partial disorder) to defective fluorite (complete disorder) phase occurs. The unit cell free volume significantly decreases due to partial substitution of small Dy^{3+} for large Sm^{3+} cations. Thus, the activation energy increases distinctly from 0.72 to 1.03 eV when the Dy content increases from $x = 0.3$ to 0.5. Although σ_{0g} continues to increase, the available number of oxide-ion decreases due to enhanced ion-ion interaction in the diffusion process [13]. Thus, the electrical conductivity obviously decreases, which indicates the decrease in electrical conductivity is mainly caused by the unit cell free volume. As the Dy content further increases from $x = 0.5$ to $x = 1.0$, the structure is located in the defective fluorite phase region, the unit cell free volume obviously decreases with increasing Dy content and the activation energy gradually further increases. Therefore, the drop in conductivity is mainly due to the decrease in the unit cell free volume with further increasing Dy content. It can be concluded that the electrical conductivity is dominated by the degree of structural disorder at the Dy content from $x = 0$ to 0.3, and is mainly controlled by the unit cell free volume from $x = 0.3$ to 1.0. This result is obviously different from the previous works on $Ln_2Zr_2O_7$ (*Ln*: rare earth metal) [20,27,28]. For the electrical behavior in the pyrochlore phase range, Wilde and Catlow reported that the oxygen vacancy hopping was important for the oxide ionic motion between 48*f* sites [26]. The electrical conductivity may be relatively low for the completely ordered pyrochlore phase such as $Sm_2Zr_2O_7$ as the 48*f* site is fully occupied. As the decrease in the *A*-site ionic radius generates the oxygen vacancies in the 48*f* site by a partial doping Dy, accompanying the cation disordering, the conductivity increases with the decrease in *A*-site ionic size. However, the reason for this is not clear. This discussion will clarify an origin of the drastic change of the electrical conductivity accompanying the phase transformation.

The defective fluorite-type phase is considered the completely disordered pyrochlore-type phase, and the electrical conductivity is lower than that of pyrochlore-type phase [13,14]. Therefore, it is reasonable that partially disordered $(Sm_{0.7}Dy_{0.3})_2Zr_2O_7$ locating at the position close to the phase boundary shows the maximum conductivity at the test temperature levels. It can be proposed that the unit cell free volume must be large to facilitate the oxide-ion migration while keeping the oxide-ion disorder state. Similar phenomenon was also found in $Eu_2Zr_2O_7$, which was close to the phase boundary [27].

As the electrolyte is the heart of the SOFC, it should be a purely ionic conduction with negligible electronic conduction at different oxygen partial pressures. Therefore, it is indispensable to measure the conductivity in reducing atmosphere. In the present study, the grain conductivity of $(Sm_{0.7}Dy_{0.3})_2Zr_2O_7$ selected as a representative in the series is investigated under the conditions of two extreme oxygen partial pressures, e.g., air and H_2 atmospheres. Fig. 10 shows the Arrhenius plots of the grain conductivity of

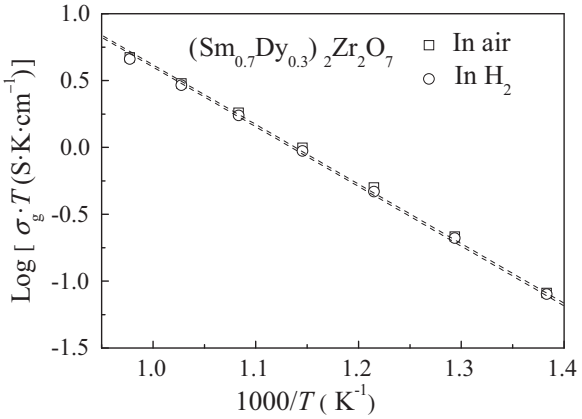

Fig. 10. Arrhenius plots of grain conductivity of $(Sm_{0.7}Dy_{0.3})_2Zr_2O_7$ ceramic in different atmospheres of air and H_2.

Table 3
Electrical property of $(Sm_{0.7}Dy_{0.3})_2Zr_2O_7$ measured in atmospheres of air and H_2.

Grain conductivity ($S\,cm^{-1}$)					
773 K		873 K		973 K	
Air	H_2	Air	H_2	Air	H_2
2.79×10^{-4}	2.71×10^{-4}	1.13×10^{-3}	1.08×10^{-3}	3.08×10^{-3}	2.99×10^{-3}

$(Sm_{0.7}Dy_{0.3})_2Zr_2O_7$ in atmospheres of air and H_2 in the temperature range of 673–1023 K. In Fig. 10, the grain conductivity of $(Sm_{0.7}Dy_{0.3})_2Zr_2O_7$ in the reducing atmosphere of H_2 is almost the same as the values obtained in air (Table 3). In fact, similar results are obtained for the remaining $(Sm_{1-x}Dy_x)_2Zr_2O_7$ ceramics. In this case, electronic conduction to the grain conductivity is negligible for $(Sm_{1-x}Dy_x)_2Zr_2O_7$ ceramics. Similar results were also reported in $(Nd_{1-y}Gd_y)_2Zr_2O_7$ systems [28]. In this investigation, Dy^{3+}, Sm^{3+} and Zr^{4+} cations are stable in H_2 atmosphere till the measurement temperature is at 1023 K. Thus, the conduction of $(Sm_{1-x}Dy_x)_2Zr_2O_7$ ceramics is purely ionic with negligible electronic conduction.

4. Conclusions

$(Sm_{1-x}Dy_x)_2Zr_2O_7$ $(0 \le x \le 0.3)$ ceramics exhibit a pyrochlore-type structure. However, $(Sm_{1-x}Dy_x)_2Zr_2O_7$ $(0.5 \le x \le 1.0)$ have a defective fluorite-type structure. The degree of structural disorder gradually increases as the Dy content increases in $(Sm_{1-x}Dy_x)_2Zr_2O_7$. The grain conductivity and total conductivity of $(Sm_{1-x}Dy_x)_2Zr_2O_7$ ceramics vary with the Dy content, and show a maximum at the Dy content of $x = 0.3$ at identical temperature levels. The factors affecting the electrical conductivity are variable depending on the Dy content. Both the activation energy E_g and the pre-exponential factor σ_{0g} for the grain conductivity gradually increase as the Dy content increases. $(Sm_{1-x}Dy_x)_2Zr_2O_7$ ceramics possess only oxide-ion conduction, and no electronic conduction is introduced.

Acknowledgement

The authors would like to thank financial support from the National Natural Science Foundation of China (NSFC-No.50972030 and 51021002).

References

[1] M.A. Subramanian, G. Aravamudan, G.V. Subba Rao, Prog. Solid State Chem. 15 (1983) 55–143.
[2] M.A. Subramanian, A.P. Ramirez, G.H. Kwei, Solid State Ionics 108 (1998) 185–191.
[3] P.K. Moon, H.L. Tuller, Solid State Ionics 28–30 (1988) 470–474.
[4] X.-L. Xia, S. Gao, Z.-G. Liu, J.-H. Ouyang, Electrochim. Acta 55 (2010) 5301–5306.
[5] J.A. Díaz-Guillén, M.R. Díaz-Guillén, J.M. Almanza, A.F. Fuentes, J. Santamaría, C. León, J. Phys.: Condens. Matter 19 (2007) 356212.
[6] J.A. Díaz-Guillén, M.R. Díaz-Guillén, J.M. Almanza, A.F. Fuentes, J. Santamaría, C. León, Solid State Ionics 179 (2008) 2160–2164.
[7] K. Shinozaki, M. Miyauchi, K. Kuroda, O. Sakurai, N. Mizutani, M. Kato, J. Am. Ceram. Soc. 62 (1979) 538–539.
[8] X.-L. Xia, J.-H. Ouyang, Z.-G. Liu, J. Power Sources 189 (2009) 888–893.
[9] B.P. Mandal, S.K. Deshpande, A.K. Tyagi, J. Mater. Res. 23 (2008) 911–916.
[10] Z.-G. Liu, J.-H. Ouyang, Y. Zhou, X.-L. Xia, J. Power Sources 185 (2008) 876–880.
[11] X.-L. Xia, J.-H. Ouyang, Z.-G. Liu, J. Am. Ceram. Soc. 93 (2010) 1074–1080.
[12] B.J. Wuensch, K.W. Eberman, C. Heremans, E.M. Ku, P. Onnerud, E.M.E. Yeo, S.M. Haile, J.K. Stalick, J.D. Jorgensen, Solid State Ionics 129 (2000) 111–133.
[13] Z.-G. Liu, J.-H. Ouyang, Y. Zhou, X.-L. Xia, Electrochim. Acta 54 (2009) 3968–3971.
[14] X.-L. Xia, J.-H. Ouyang, Z.-G. Liu, S. Gao, S. Li, J. Electrochem. Soc. 157 (2010) B470–B476.
[15] Z.-G. Liu, J.-H. Ouyang, Y. Zhou, J. Li, X.-L. Xia, Int. J. Appl. Ceram. Technol. 6 (2009) 485–491.
[16] Z.-G. Liu, J.-H. Ouyang, Y. Zhou, J. Li, X.-L. Xia, J. Eur. Ceram. Soc. 29 (2009) 647–652.
[17] K.R. Whittle, L.M.D. Cranswick, S.A.T. Redfern, I.P. Swainson, G.R. Lumpkin, J. Solid State Chem. 182 (2009) 442–450.
[18] G.S. Rohrer, Structure and Bonding in Crystalline Materials, Cambridge University Press, Cambridge, 2004, pp. 521–525.
[19] M.T. Vandenborre, E. Husson, J.P. Chatry, D. Michel, J. Raman Spectrosc. 14 (1983) 63–71.
[20] B.P. Mandal, A. Banerjib, V. Sathec, S.K. Debb, A.K. Tyagia, J. Solid State Chem. 180 (2007) 2643–2648.
[21] M. Glerup, O.F. Nielsen, F.W. Poulsen, J. Solid State Chem. 160 (2001) 25–32.
[22] J.R. Macdonald, W.B. Johnson, in: E. vBarsoukov, J.R. Macdonald (Eds.), Impedance Spectroscopy: Theory, Experiment and Applications, 2nd ed., John Wiley & Sons, Inc., New Jersey, 2005 (Chapter 1).
[23] B.A. Boukamp, Equivalent Circuit (Equivcrt. Pas) Users Manual, 2nd ed., Twente University, The Netherlands, 1989.
[24] H. Yamamura, K. Matsui, K. Kakinuma, T. Mori, Solid State Ionics 123 (1999) 279–285.
[25] H. Nishino, N. Matsunaga, K. Kakinuma, H. Yamamura, K. Nomura, J. Ceram. Soc. Jpn. 112 (2004) S738–S741.
[26] P.J. Wilde, C.R.A. Catlow, Solid State Ionics 112 (1998) 173–183.
[27] H. Yamamura, H. Nishino, K. Kakinuma, K. Nomura, Solid State Ionics 158 (2003) 359–365.
[28] B.P. Mandal, A. Dutta, S.K. Desppande, R.N. Basu, A.K. Tyagi, J. Mater. Res. 24 (2009) 2855–2862.